A benchmark study of the multiscale and homogenization methods for fully implicit multiphase ow simulations with adaptive dynamic mesh (ADM)

H. Hajibeygi, M. Bastidas Olivares, M. HosseiniMehr, I.S. Pop, M.F. Wheeler

UHasselt Computational Mathematics Preprint
Nr. UP-19-08

Oct. 10, 2019

A benchmark study of the multiscale and homogenization methods for fully implicit multiphase flow simulations with adaptive dynamic mesh (ADM)

Hadi Hajibeygi[a,*], Manuela Bastidas Olivares[b], Mousa HosseiniMehr[a], Sorin Pop[b], Mary Wheeler[c]

[a] *Faculty of Civil Engineering and Geosciences, Delft University of Technology, P.O. Box 5048, 2600 GA Delft, the Netherlands.*
[b] *Faculty of Sciences, Hasselt University, Diepenbeek, Belgium*
[c] *Institute for Computational Engineering and Sciences, The University of Texas at Austin, 201 East 24th Street, ACE 5.324, Campus Mail C0200, Austin, TX 78712*

Abstract

Accurate simulation of multiphase flow in subsurface formations is challenging, as the formations span large length scales (km) with high resolution heterogeneous properties. To deal with this challenge, different multiscale methods have been developed. Such methods construct coarse-scale systems, based on a given high-resolution fine-scale system. Furthermore, they are amenable for parallel computing, and allow for a posterior error control. When bridging the gap between the different scales, these methods differ significantly from each other. One type of multiscale methods compute local basis functions to map the solution; instead, homogenization methods consider (locally) periodic call problems to determine the effective parameters at the relevant scale. It is yet unknown how these two methods compare with each other, especially when applied to complex geological formations, with no separation of scales in the property fields. This paper develops the first comparison benchmark study of these two methods, and extends their applicability to fully implicit dynamic multilevel (ADM) simulations. At each time step, on the given fine-scale mesh and based on an error analysis, the fully implicit system is solved on a dynamic multilevel grid. The entries of this system are obtained by using multiscale local basis functions (ADM-MS), and, respectively, by parameter homogenization over local domains (ADM-HO). Both sets of local basis functions (ADM-MS) and local effective parameters (ADM-HO) are computed at the beginning of the simulation, with no further updates during the multiphase flow simulation. The two methods are extended and implemented in the same open-source DARSim2 simulator (https://gitlab.com/darsim2simulator), to provide a fair quality comparison for the different test cases. The results reveal insightful understanding of the two approaches, and benchmarks the quality of their results for the given scenarios. In particular, it is reemphasized that the test cases considered here include permeability fields with no clear scale separation. The development of this paper sheds new lights on advanced multiscale methods for simulation of coupled processes in porous media.

Keywords: Multiscale, Homogenization, Algebraic dynamic multilevel, Multilevel multiscale, Adaptive mesh refinement, Porous media, Multiphase flow, Fully implicit simulation, Reservoir simulation

1. Introduction

Geological formations span large (km) length scales, having heterogeneous properties characterized at high resolutions (cm and below). As for the uncertainty within the integrated field data, several realizations of equiprobable property fields are typically generated to study and simulate the fluid flow dynamics within the formations. Classical simulation approaches are too expensive for these studies. Therefore, advanced simulation methods are required to allow for accurate representation of the heterogeneous properties, and, at the same time, provide efficient simulation framework to study multiple realizations [31, 33].

Model order reduction techniques have been developed to provide meaningful approximate simulation framework, in the sense that they are fast to be obtained for large-scale computational domains. Note that any advanced method of this type becomes field applicable only when it allows for error reduction to any desired threshold value [26].

Within the model order reduction techniques, two promising developments for next-generation simulators are (1) multiscale [23, 30] and (2) homogenization (or upscaling) [19] methods.

These approaches are different in the sense that the former method (multiscale) deals with crossing the solution (e.g. pressure) across the scales [1, 32, 25, 14], while the latter (homogenization) aims at development of effective lower-resolution parameters (e.g. permeability or transmissibility) [20, 3, 21]. Moreover, multiscale basis functions have been formulated purely algebraic [43], while the same does not hold for homogenized (and other parameter-

*Corresponding author
Email addresses: H.Hajibeygi@tudelft.nl (Hadi Hajibeygi), manuela.bastidas@uhasselt.be (Manuela Bastidas Olivares), S.Hosseinimehr@tudelft.nl (Mousa HosseiniMehr), sorin.pop@uhasselt.be (Sorin Pop), mfw@ices.utexas.edu (Mary Wheeler)

based upscaling e.g. flow-based upscaling) parameters. Specially integration of homogenized parameters within the fully implicit framework in an algebraic manner has not yet been developed so far. The developments of this work includes this achievement too.

Both methods, at the same time, have many similarities. Both find their mapping strategy via local solutions of the original governing equations with local boundary conditions. Multiscale basis functions often times employ reduced-dimensional boundary conditions [42, 34], and the homogenization schemes employ periodic boundary conditions [5, 2]. Both methods are effective for global equations within the fully coupled system of local-global unknowns (e.g. global pressure and local saturation). Both have been extended to nonlinear and geologically complex models [6, 29, 40]. Recent developments of these two classes of approaches have introduced fully-implicit dynamic multilevel simulation framework (ADM) in which heterogeneous detailed geo-models are mapped into adaptive dynamic coarser mesh [15, 24].

The ADM method develops a fully-implicit discrete system for coupled flow and transport equations in which each equation can be represented at different resolution than the defined fine-scale one. More importantly, the procedure can be done fully algebraic based on an error threshold. In contrast to the rich existing literature on Adaptive Mesh Refinement (AMR) methods [10, 35, 11, 38, 22, 37], ADM can be defined as an adaptive mesh coarsening strategy which is automatically applicable to heterogeneous and coupled systems [17].

Irrespective of the choice of the dynamic mesh strategy, it is always a challenge to construct adaptive multiscale entries of the implicit systems.
The ADM method so far has included multiscale basis functions [17]. Following ADM development, homogenisation methods have been also developed for dynamic grids [6, 16]. Of great interest to the scientific community is the investigation of the homogenisation-based coarser system entries, and a benchmark study of the quality of the two approaches of ADM-multiscale (ADM-MS) and ADM-homogenized (ADM-HO) for coupled implicit multiphase flow scenarios.

This paper develops such a unified framework, in which ADM method is extended to account for both multiscale and homogenisation schemes for multiphase flow simulations. This development makes it possible to allow for different coarse-scale entries for dynamic simulations, and importantly to benchmark the two classes of multiscale and homogenization strategies. Important is that, once the effective parameters are computed, all other homogenization procedures are implemented algebraically. This is done by introducing constant unity local basis, with the support of primal (non-overlapping) coarse-scale partitions. The multiscale ADM is implemented fully algebraic, since local basis functions are also solved algebraically over the overlapping (dual) coarse grid domains [44]. Our development is made available to the public via an open-source DARSim2 simulator, https://gitlab.com/darsim2simulator.

Numerical test cases are considered for the challenging highly heterogeneous SPE10 [13] and periodic fields. These allow one to realise how homogenisation (or upscaling) strategies would perform on field-relevant test cases. The number of active grid cells, pressure and saturation errors, and the solution maps are all reported in details. The development of this paper sets a new light in application of multiscale and upscaling (i.e. homogenization) approaches in advanced next-generation environments for field-relevant simulation scenarios.

The paper is structured as follows. Next, in Section 2, the governing equations are briefly revisited. Section 3 presents the computational framework for both multiscale and homogenization ADM methods. Section 4 presents the test cases and finally the paper is concluded in Section 5.

2. Governing equations

Mass balance for two-phase flow in porous media at continuum (Darcy) scale reads

$$\frac{\partial}{\partial t}(\phi\rho_i S_i) - \nabla\cdot(\rho_i\lambda_i\cdot(\nabla p - \rho_i g\nabla z)) = \rho_i q_i,\ \ \forall i\in\{\alpha,\beta\}. \tag{1}$$

Here, ϕ is the porous medium porosity, ρ [kg/m^2] is the phase density and S is the phase saturation. The phase mobility λ is equal to KKr_i/μ_i, where K [m^2] is the rock permeability, Kr_i is the phase relative permeability (function of phase saturation) and μ [Pa.s] is the phase viscosity. In addition, p [Pa] is the pressure, g [m/s^2] is the gravitational acceleration which acts on ∇z direction and q [1/s] is the phase source term. The constraint of $S_\alpha + S_\beta = 1$ makes the above equations well-posed for 2 unknowns of S_α (in short from here on, S) and p.

The fully-implicit coupled simulation approach [8] estimates all the parameters at next time step $(n+1)$. As such, the semi-discrete nonlinear residual for the phase $i\in\{\alpha,\beta\}$ reads

$$\begin{aligned} R_i^{n+1} = \ & [\rho_i q_i]^{n+1} - \frac{(\phi\rho_i S_i)^{n+1} - (\phi\rho_i S_i)^n}{\Delta t} \\ & +\nabla\cdot(\rho_i\lambda_i\cdot(\nabla p - \rho_i g\nabla z))^{n+1}. \end{aligned} \tag{2}$$

For finding the solution pair (p^{n+1}, S^{n+1}) one needs to employ a linearization scheme. Here we restrict the discussion to the Newton scheme, which is 2nd-order convergent, but requires a starting point that is close enough to the solution. In other words, the time step may be subject to restrictions depending also on the mesh size. Alternatively, one may consider approaches like the modified Picard [12] or the L-Scheme [36], which are less demanding from computational point of view, or more robust w.r.t. the starting point or the discretization mesh, but converge

slower than the Newton scheme. Such schemes are analyzed in [9] in multiscale framework. Applied to (2), the Newton linearization reads

$$R^{n+1} \approx R^{\nu} + \frac{\partial R}{\partial p}|^{\nu} \delta p^{\nu+1} + \frac{\partial R}{\partial S}|^{\nu} \delta S^{\nu+1}, \tag{3}$$

through solving linear system $\mathbf{J}^{\nu}\delta\mathbf{x}^{\nu+1} = -\mathbf{R}^{\nu}$, i.e.,

$$\underbrace{\begin{bmatrix} \frac{\partial R_\alpha}{\partial p} & \frac{\partial R_\alpha}{\partial S} \\ \frac{\partial R_\beta}{\partial p} & \frac{\partial R_\beta}{\partial S} \end{bmatrix}^{\nu}}_{\mathbf{J}} \underbrace{\begin{bmatrix} \delta p \\ \delta S \end{bmatrix}^{\nu+1}}_{\delta\mathbf{x}} = -\underbrace{\begin{bmatrix} R_\alpha \\ R_\beta \end{bmatrix}^{\nu}}_{\mathbf{R}} \tag{4}$$

In each time step, the linear Eq. (4) is solved iteratively (inner loop) several times until nonlinear convergence (outer loop) is reached. It is clear that the computational complexity of the simulation depends highly on the complexity of the solution of this linear system. Advanced multiscale and homogenization methods aim at solving this linear system on a dynamic multilevel mesh. Note that, as shown before [15], the overall efficiency of any advanced method should include not only the speedup of solving the linear Eq. (4) but also the count of the Newton (outer) loops. Next, the ADM method based on multiscale and homogenisation formulations is presented.

3. Dynamic Multilevel Simulation based on Multiscale and Homogenization Methods

3.1. ADM framework formulation

The fully-implicit linear system (4) at fine scale is too expensive to be solved for real field scenarios. A multilevel dynamic mesh, as shown in Figure 1, is generated within ADM framework, based on an error estimate strategy. The error estimate is developed based on a front tracking criterion, i.e., it leads to employment of fine-scale grids only at sub-regions with sharp gradients. The fine-scale system is then algebraically reduced into this multilevel grid, through sequences of restriction and prolongation operators. As the first step to obtain the ADM grid, sets of $N^l = N_x^l \times N_y^l$ hierarchically nested coarse grids are imposed on the fine-scale computational domain. Here, l indicates the coarsening level and γ^l is the coarsening ratio which is defined as

$$\gamma^l = (\gamma_x^l, \gamma_y^l) = (\frac{N_x^{l-1}}{N_x^l}, \frac{N_y^{l-1}}{N_y^l}), \tag{5}$$

for two-dimensional (2D) domains. The ADM grid is constructed by assembling a combination of grid-cells at different resolutions within a computational domain. By using the sequence of restriction ($\mathbf{R}$) and prolongation ($\mathbf{P}$) operators, one can express the ADM system as

$$\underbrace{\hat{\mathbf{R}}_l^{l-1} \dots \hat{\mathbf{R}}_1^0 \, \mathbf{J_0} \, \hat{\mathbf{P}}_0^1 \dots \hat{\mathbf{P}}_{l-1}^l}_{\mathbf{J}_{\mathrm{ADM}}} \delta\hat{x}_{\mathrm{ADM}} = -\underbrace{\hat{\mathbf{R}}_l^{l-1} \dots \hat{\mathbf{R}}_1^0 \, r_0}_{\hat{\mathbf{R}}_{\mathrm{ADM}}}. \tag{6}$$

Here, $\hat{\mathbf{R}}_l^{l-1}$ is the restriction operator which maps the parts of the solution vector that are at level $l-1$ to level l. Similarly, the prolongation operator $\hat{\mathbf{P}}_{l-1}^l$ maps the parts of the solution vector that are at level l to level $l-1$. Once the ADM system (6) is solved, on the multilevel mesh, the approximated fine-scale solution ($\delta x_0'$) can be acquired by prolonging the ADM solution ($\delta\hat{x}_{\mathrm{ADM}}$) i.e.

$$\delta x_0 \approx \delta x_0' = \hat{\mathbf{P}}_0^1 \dots \hat{\mathbf{P}}_{l-1}^l \, \delta x_{\mathrm{ADM}}. \tag{7}$$

The ADM Restriction ($\hat{\mathbf{R}}_l^{l-1}$) and prolongation ($\hat{\mathbf{P}}_{l-1}^l$) operators are assembled using the static multilevel multiscale restriction ($\mathbf{R}_l^{l-1}$) and prolongation ($\mathbf{P}_{l-1}^l$) operators respectively. They are constructed only at the beginning of the simulation and are kept unchanged throughout the entire simulation.

The static prolongation operator $\mathbf{P}_{l-1}^l$ is constructed as an assembly of the locally computed basis functions at each coarsening level l and reads

$$\mathbf{P}_{l-1}^l = \begin{pmatrix} (P_p)_{l-1}^l & 0 \\ 0 & (P_S)_{l-1}^l \end{pmatrix}_{N_{l-1} \times N_l}. \tag{8}$$

Here, $(P_p)_{l-1}^l$ and $(P_S)_{l-1}^l$ are the two main diagonal blocks corresponding to main unknowns (i.e., pressure p and saturation S). In case of using homogenisation scheme (i.e., ADM-HO, as will be described in Section 3.3), constant basis functions for pressure are used. However, for multiscale-based ADM (i.e., ADM-MS, as will be described in Section 3.2) locally computed basis functions are used. Note that the saturation prolongation operator for both approaches are constant to unity function at all coarsening levels, which represents the conservative finite-volume integration.

The static restriction operator $\mathbf{R}_l^{l-1}$ reads

$$\mathbf{R}_{l-1}^l = \begin{pmatrix} (R)_{l-1}^l & 0 \\ 0 & (R)_{l-1}^l \end{pmatrix}_{N_{l-1} \times N_l}. \tag{9}$$

In this work, finite-volume restriction operator is used to guarantee local mass conservation, i.e.,

$$R_l^{l-1}(i,j) = \begin{cases} 1 & \text{if cell } i \text{ is inside coarser cell } j, \\ 0 & \text{otherwise.} \end{cases} \tag{10}$$

3.2. ADM using multiscale (ADM-MS)

In ADM-MS method, the prolongation operator for pressure is found based on multiscale basis functions. These local basis functions are computed algebraically [43], based on the pressure equation. In this study, the incompressible flow equation (elliptic pressure equation) is used to construct the multiscale basis functions [42]. An example of a basis function is shown in Figure 2.

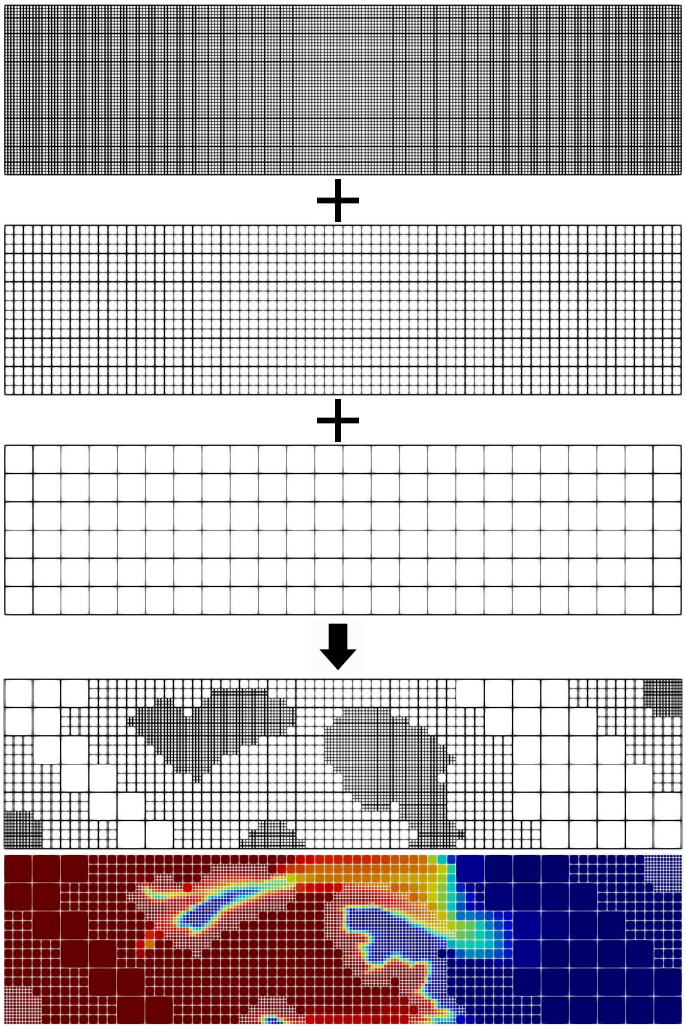

Figure 1: Example of a ADM solution grid combining fine-scale resolution with 2 coarsening level. The three figures on top are the grid structure at fine-scale, coarse level 1 and coarse level 2 resolution. The figure below these three figures, show an ADM grid constructed by the combination of these hierarchically nested grids. Lastly, the figure at the very bottom is the saturation profile corresponding to that ADM grid.

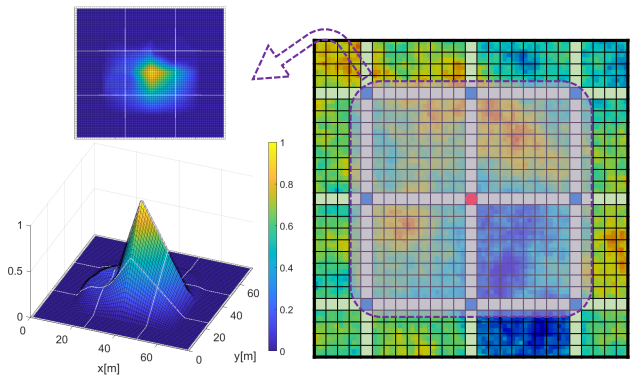

Figure 2: An example of a basis function belonging to the middle coarse node of a heterogeneous 2D domain.

3.3. ADM using homogenization (ADM-HO)

Homogenization method can be used to construct the effective properties at the dynamic multilevel mesh. The effective properties at multilevel mesh are found (similar as in ADM-MS) by solving local flow (pressure) equations based on incompressible (elliptic) equation.

To develop ADM-HO system, a scale separation is assumed. Further, by doubling the spatial variable into a fast and a slow one, one assumes that all quantities in Eq. (1) satisfy the *homogenization ansatz* theory, namely that they can be expanded regularly in terms of the scale separation parameter and they are locally periodic w.r.t. the fast variable. For theoretical details we refer to [28, 5, 18], and to [4, 39, 7, 9, 41, 27] where these ideas are used to develop effective numerical simulation schemes.

In a simplified framework, at each ADM level an effective permeability tensor $\mathbf{K}^l$ is computed locally for each coarse cell Ω^l and at level l as

$$\mathbf{K}^l_{i,j}\Big|_{\Omega^l} = \int_{\Omega^l} \left(K\ \left(\mathbf{e}_j + \nabla\omega^j\right)\right) \cdot \mathbf{e}_i\, d\mathbf{y}. \tag{11}$$

Here ω^j are the periodic solutions of the *micro-cell* equation, which can be expressed as

$$-\nabla \cdot \left(K\ \left(\nabla_y \omega^j + \mathbf{e}_j\right)\right) = 0, \text{ for all } \mathbf{y} \in \Omega^l. \tag{12}$$

Here $\{\mathbf{e}_j\}_{j=1}^d$ is the canonical basis of dimension d. To guarantee the uniqueness of the solution ω^j, next to its periodicity, one assumes that the average value over the cell Ω^l is 0.

To determine the value of the permeability tensor at each coarse cell Ω^l, two micro-cell problems (12) are solved for each spatial direction in 2D. Figure 3 provides an illustration of these local solutions for a coarse element.

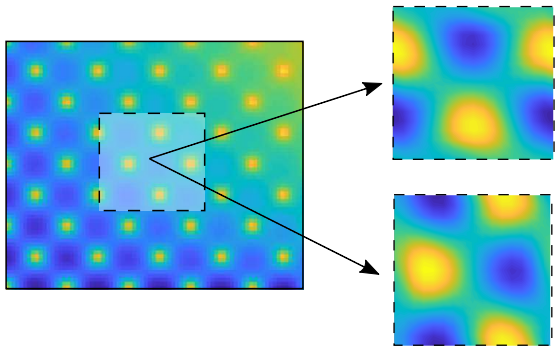

Figure 3: Example of the local solutions ω^x (top right, for x-direction) and ω^y (bottom right, for y-direction) for a coarse cell inside a 2D domain. The heterogeneous permeability field is also shown for the entire domain (left).

Note that the local problems (12) capture the rapidly oscillating characteristics within a coarse element, completely decoupled from other coarse elements. The homogenized parameters, like multiscale bases, are computed at the beginning of the simulation. Figure 4 illustrates the calculation of the effective permeability at different levels.

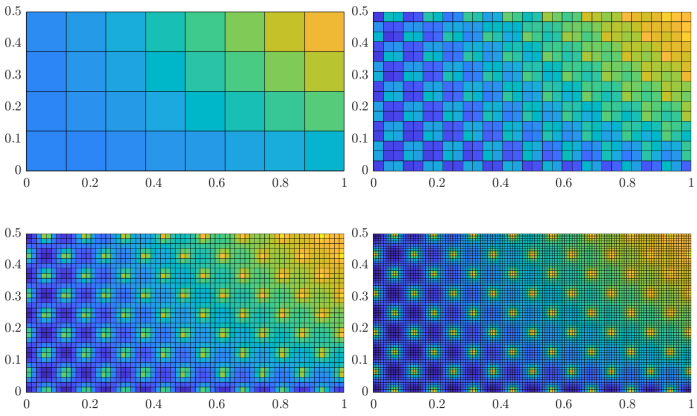

Figure 4: Example of four different levels of homogenized permeability values: fine scale (bottom right), coarse level 1 (bottom left), coarse level 2 (top right) and coarse level 3 (top left).

Given a fine-scale permeability field K and the coarsening ratios γ^l, the effective permeability tensors are computed. These values will be used for construction of coarse-scale system at a given sub-domain. Moreover, when the homogenized parameters are used, constant unity functions are employed to interpolate the coarse-scale solutions to the fine-scale ones. This is achieved by setting prolongation operators in Eq. (6) to unity.

4. Simulation results

To benchmark the homogenization and multiscale based solutions for dynamic mesh on heterogeneous media, two heterogeneous non-periodic permeability fields from the top and bottom layers of the SPE 10th Comparative Solution Project [13] are considered. For both test cases, the computational domain entails 216×54 grid cells at fine-scale with $\Delta x = \Delta y = 1$[m]. No-flow condition is imposed on all boundaries. Reservoir initially contains oil and Water is injected from the injection well. Both fluids are assumed to be incompressible. Injection and production take place through introducing source terms (wells).

Table 1 shows the input parameters of the fluid and rock properties used in all test cases.

Table 1: Input parameters of fluid and rock properties.

Property	value
Porosity (ϕ)	0.2
Water density (ρ_w)	1000 [Kg/m^3]
Oil density (ρ_o)	1000 [Kg/m^3]
Water viscosity (μ_w)	10^{-3} [Pa·s]
Oil viscosity (μ_o)	10^{-3} [Pa·s]
Initial pressure (p_0)	10^7 [Pa]
Connate water saturation (S_{wc})	0 [-]
Residual oil saturation (S_{or})	0 [-]
Injection pressure (p_{inj})	2×10^7 [Pa]
Production pressure (p_{prod})	0 [Pa]

Numerical results of ADM-MS and ADM-HO methods will be compared to those obtained from fine-scale reference permeability simulations. Both ADM methods employ the coarsening ratio of 3×3 with two coarsening levels. This is set due to the size of the domain.

4.1. Test case 1: SPE10 top layer

In this test case, one injection well and one production well are placed in the bottom left corner and top right corner of the domain, respectively. The simulation time is $t = 1000$ [days] and the results are reported on 100 equidistant time intervals.

The permeability distribution of the SPE10 top layer is shown in Figure 5.

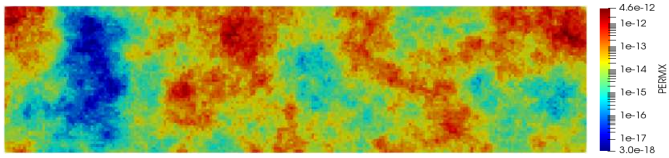

Figure 5: Fine-scale permeability (Log_{10} scale) from top layer of the SPE10 dataset.

Figure 6 shows the homogenized version of the permeability at 2 different levels. We highlight that the homogenized permeability at both coarse levels preserve the structure of the original fine-scale permeability. The high and low permeable zones remain clearly detectable.

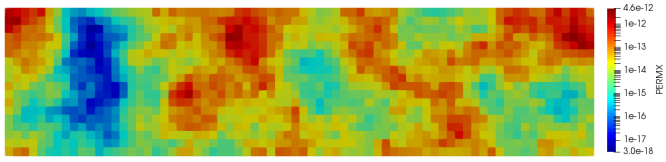

(a) Level 1 (72×18 cells).

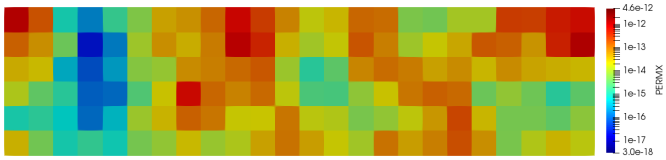

(b) Level 2 (24×6 cells).

Figure 6: Homogenized permeability of the top layer of the SPE10 with coarsening ratio 3.

The saturation and pressure fields at the final time step are shown in Figure 7 and Figure 8, respectively.

Using an effective homogenized parameter for a coarse cell with high and low permeable fine cells can lead to higher flow leakage, compared with fine-scale and multiscale-based approaches. This effect can be seen in Figure 7. Figure 9 illustrates the adaptive mesh at 2000 days after injection. Notice that the refinement of the permeability is mostly dominant at the saturation front, due to the chosen mesh refinement criterion. For this figure, the coarsening

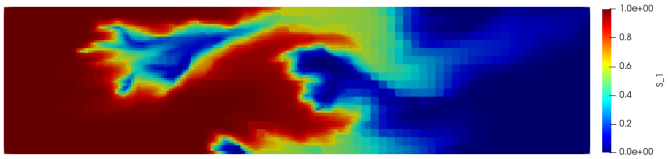

(a) ADM using homogenized permeabilities.

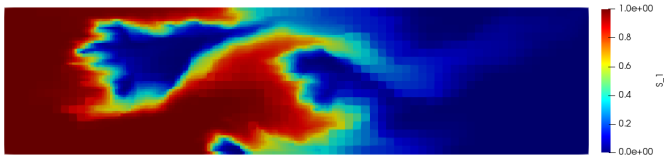

(b) ADM using multi-scale basis functions.

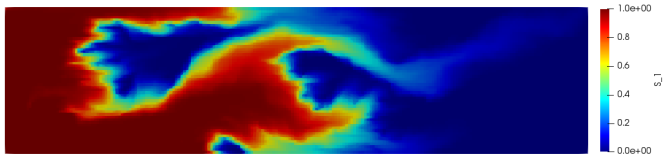

(c) Fine-scale (Reference solution).

Figure 7: Saturation profiles at 2000 days. The threshold value for the front tracking criterion is $\Delta S = 0.3$.

(a) ADM using homogenized permeabilities.

(b) ADM using multi-scale basis functions.

(c) Fine-scale (Reference solution).

Figure 8: Pressure profiles at 2000 days. The threshold value for the front tracking criterion is $\Delta S = 0.3$.

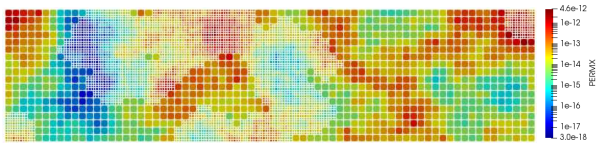

Figure 9: Adaptive mesh and homogenized permeability for the SPE10 top layer test case. The threshold value for the front tracking criterion is $\Delta S = 0.3$.

threshold value is $\Delta S = 0.3$, i.e. a cell is successively coarsened if ΔS is lower than 0.3.

The error history maps for ADM-MS and ADM-HO are shown in Figure 10. The relative errors, presented in Figure 10 and Figure 12, are calculated with respect to the fine-scale solution as

$$Error(S) = \frac{\|S_{\text{ref}} - S_{\text{ADM}}\|_2}{\|S_{\text{ref}}\|_2} \tag{13}$$

$$Error(P) = \frac{\|P_{\text{ref}} - P_{\text{ADM}}\|_2}{\|P_{\text{ref}}\|_2}. \tag{14}$$

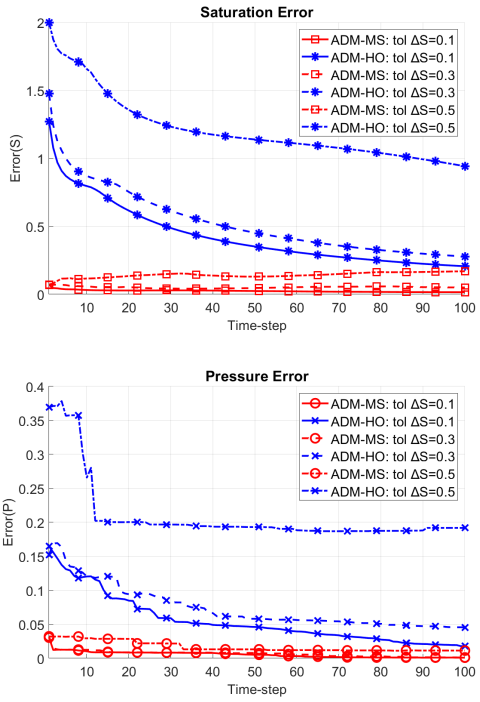

Figure 10: Comparison of the saturation and pressure error using ADM-MS and ADM-HO and 3 different values for the front tracking criterion.

The results indicate that the homogenization-based simulations have higher errors compared with the multiscale-based simulations. They both have similar average usage of active grid cells, with ADM-MS having slightly fewer grid cells. This is shown in Figure 11. Note that grid cells around wells are kept at the fine-scale resolution permanently. Furthermore, for tighter error tolerance values, the quality of the both approaches become comparable.

Figure 12 provides the average pressure and saturation errors together with the average percentage of active grid cells during the whole simulation time as functions of the coarsening criterion threshold.

4.2. Test case 2: SPE10 bottom layer

The permeability distribution of the SPE10 bottom layer is considered as the second test case. The location of the injection and production wells are the top left and the bottom right corners, respectively. The simulation time is

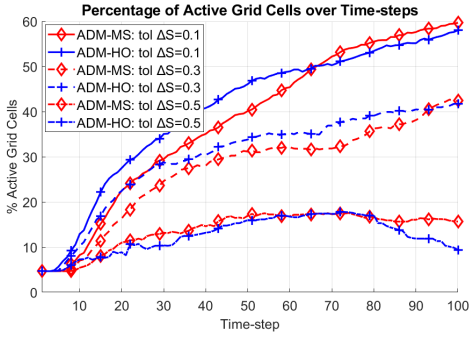

Figure 11: Comparison of the active grid cells using ADM-MS and ADM-HO and 3 different values for the front tracking criterion.

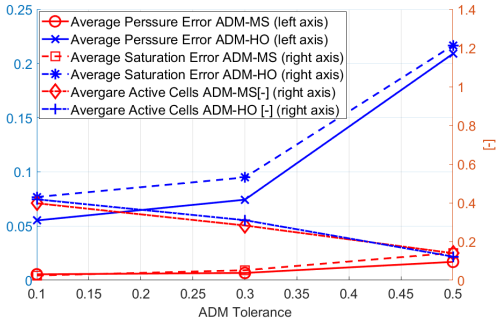

Figure 12: Average errors for the pressure and saturation and average active grid cells for each strategy (ADM-MS and ADM-HO).

20 [days]. All other simulation parameters are identical to the first test case.

The permeability distribution of the SPE10 bottom layer is shown in Figure 13.

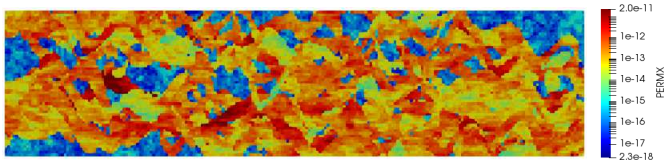

Figure 13: Fine-scale permeability (Log_{10} scale) from bottom layer of the SPE10 test case.

Figure 14 shows the homogenized permeability values at 2 different levels. In this case, the channelized patterns of the permeability are less visible. Due to the many high contrast channels, more active cells are employed compared with the SPE top layer, as shown in Figure 15.

The saturation and pressure maps at the final time step are shown in Figure 16 and Figure 17, respectively.

Similar to previous test cases, Figure 18 compares the error between the two ADM approaches. Moreover, in Figure 19 the percentage of active grid cells per each time-step is shown.

Figure 20 illustrates average values of pressure and saturation errors, and percentage of active grid cells for each coarsening criterion threshold.

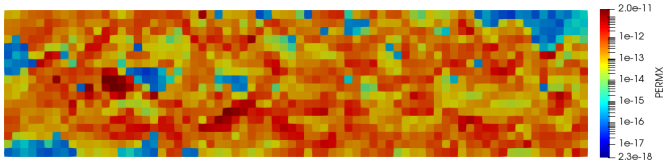

(a) Level 1 (72×18 cells).

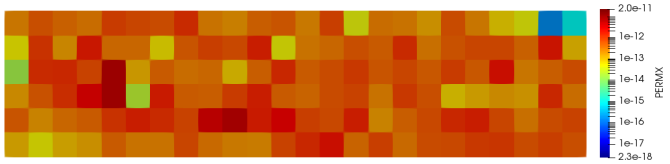

(b) Level 2 (24×6 cells).

Figure 14: Homogenized permeability of the SPE10 bottom layer with coarsening ratio 3.

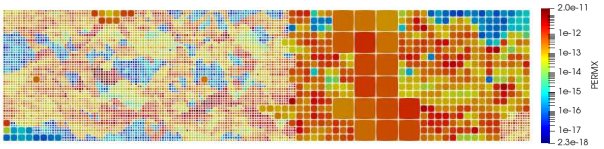

Figure 15: Refinement of the permeability of the bottom layer of the SPE10 using ADM-HO after 20 days. The threshold value for the front tracking criterion is $\Delta S = 0.3$.

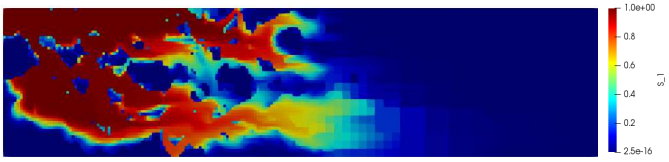

(a) ADM using homogenized permeabilities.

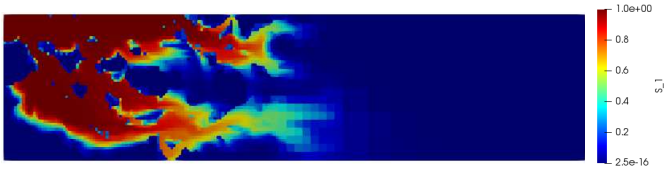

(b) ADM using multi-scale basis functions.

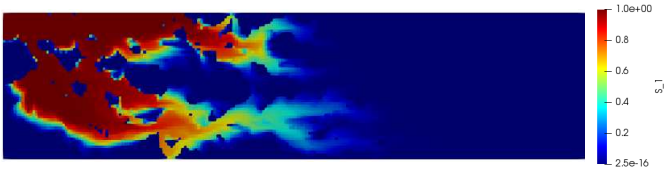

(c) Fine-scale (Reference solution).

Figure 16: Saturation profiles at 20 days. The threshold value for the front tracking criterion is $\Delta S = 0.3$.

(a) ADM using homogenized permeabilities.

(b) ADM using multi-scale basis functions.

(c) Fine-scale (Reference solution).

Figure 17: Pressure profiles at 20 days. The threshold value for the front tracking criterion is $\Delta S = 0.3$.

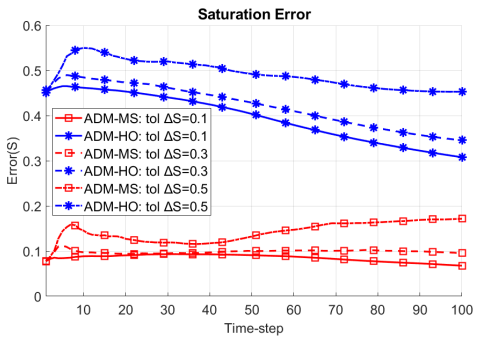

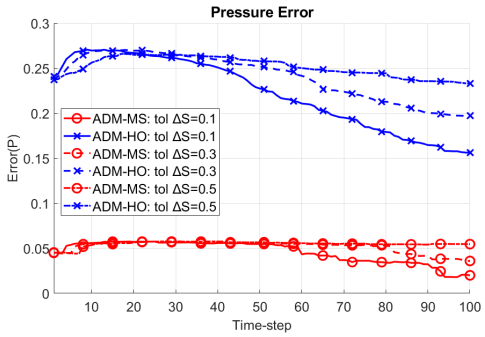

Figure 18: Comparison of the saturation and pressure error using ADM-MS and ADM-HO and 3 different values for the front tracking criterion.

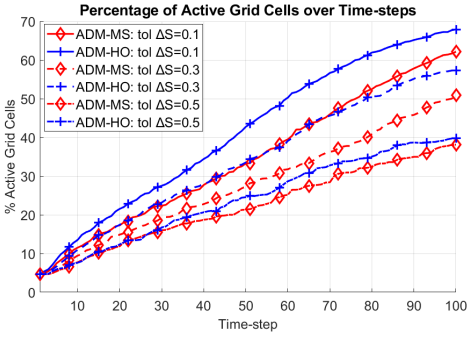

Figure 19: Comparison of the active grid cells using ADM-MS and ADM-HO and 3 different values for the front tracking criterion.

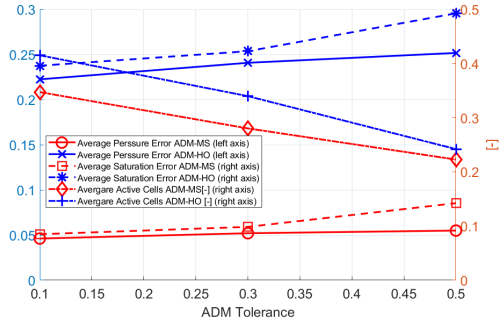

Figure 20: Average errors for the pressure and saturation and average active grid cells for both approaches (ADM-MS and ADM-HO)

The results indicate a noticeable difference in the errors of ADM-MS and ADM-HO. The pressure error in ADM-HO is significantly higher due to the fact that ADM-HO uses homogenized effective parameters, instead ADM-MS employs multisclae basis functions. Moreover, as the result of more accurate pressures, ADM-MS saturation error is lower than that of ADM-HO. The difference of the percentage of active grid cells used in the two approaches is less noticeable than the difference of the errors. However, the ADM-HO uses more active grid cells especially in this SPE10 bottom layer test case.

5. Conclusion

Homogenization and multiscale methods have been developed and evolved during the past decade as promising advanced simulation approaches for heterogeneous large-scale systems. In this work, the two methods were investigated, extended into a unified fully-implicit framework, and benchmarked for simulation of multiphase flow in porous media. It was shown that the two methods allow construction of coarser level systems, and both rely on local solutions to find their corresponding maps. While homogenization methods deliver effective parameters, multiscale methods find interpolation of the solution (pressure) across scales. This is the main difference between the two approaches. For highly heterogeneous test cases it was shown that the two approaches provide accurate so-

lutions, while ADM-MS provided more accurate solutions compared with ADM-HO. The use of effective parameters for coarse cells with high and low permeable cells can lead to excessive leakage if an effective parameter is used instead of the basis function. Furthermore, it was very important to demonstrate solutions of ADM-HO for permeability fields with no periodic structure. This illustrated the applicability of homogenization methods for problems with no separation of scales, if they are combined with an adaptive mesh strategy (ADM). Moreover, both methods were developed algebraic. Specially by setting constant unity prolongation operator, it was shown how ADM-HO can be developed in a straightforward manner. The study of this paper sheds new lights in application of multiscale and homogenization methods for real-field simulation of multiphase flow in porous media. On going study includes benchmark studies of ADM-HO and ADM-MS for 3D fractured porous media.

6. Acknowledgements

Hadi Hajibeygi was sponsored through Dutch Science Foundation (NWO) grant 17509, under Innovational Research Incentives Scheme Vidi. All authors acknowledge TU Delft DARSim group members for the fruitful discussions, specially Matteo Cusini and Jeroen Rijntjes for their helps regarding DARSim2 simulator. DARSim2 open-source simulator can be publically accessed via https://gitlab.com/darsim2simulator link.

[1] Aarnes, J., Hou, T.Y., 2002. Multiscale domain decomposition methods for elliptic problems with high aspect ratios. Acta Math. Appl. 18, 63–76.

[2] Abdulle, A., E, W., 2003. Finite difference heterogeneous multiscale method for homogenization problems. J. Comput. Phys. 191, 18–39.

[3] Abdulle, A., E, W., Engquist, B., Vanden-Eijnden, E., 2012. The heterogenous multiscale method. Acta Numer. 21, 1–87.

[4] Abdulle, A., Nonnenmacher, A., 2009. A short and versatile finite element multiscale code for homogenization problems. Computer Methods in Applied Mechanics and Engineering 198, 2839–2859.

[5] Allaire, G., 1992. Homogenization and two-scale convergence. SIAM Journal on Mathematical Analysis 23, 1482–1518. URL: https://doi.org/10.1137/0523084, doi:10.1137/0523084, arXiv:https://doi.org/10.1137/0523084.

[6] Amanbek, Y., Singh, G., Wheeler, M.F., van Duijn, H., 2019a. Adaptive numerical homogenization for upscaling single phase flow and transport. Journal of Computational Physics 387, 117 – 133. doi:https://doi.org/10.1016/j.jcp.2019.02.014.

[7] Amanbek, Y., Singh, G., Wheeler, M.F., van Duijn, H., 2019b. Adaptive numerical homogenization for upscaling single phase flow and transport. Journal of Computational Physics .

[8] Aziz, K., Settari, A., 2002. Petroleum Reservoir Simulation. Blitzprint Ltd., Cagary, Alberta.

[9] Bastidas, M., Bringedal, C., Pop, I.S., Radu, F.A., 2019. Adaptive numerical homogenization of nonlinear diffusion problems. arXiv:arXiv:1904.10665.

[10] Bell, J.B., Lijewski, M.J., Pau, G.S.H., Almgren, A.S., 2009. A parallel second-order adaptive mesh algorithm for incompressible flow in porous media. Philos. T. Roy. Soc. A 367, 4633–4654.

[11] Berger, M., Oliger, J., 1984. Adaptive mesh refinement for hyperbolic partial differential equations. J. Comput. Phys. 53, 484–512.

[12] Celia, M.A., Bouloutas, E.T., Zarba, R.L., 1990. A general mass-conservative numerical solution for the unsaturated flow equation. Water resources research 26, 1483–1496.

[13] Christie, M.A., Blunt, M.J., February, 2001. Tenth spe comparative solution project: A comparison of upscaling techniques. SPE 66599, presented at the SPE Symposium on Reservoir Simulation, Houston .

[14] Chung, E.T., Efendiev, Y., Lee, C.S., 2015. Mixed generalized multiscale finite element methods and applications. Multiscale Modeling & Simulation 13, 338–366.

[15] Cusini, M., Fryer, B., van Kruijsdijk, C., Hajibeygi, H., 2018. Algebraic dynamic multilevel method for compositional flow in heterogeneous porous media. Journal of Computational Physics 354, 593–612. doi:10.1016/j.jcp.2017.10.052.

[16] Cusini, M., Gielisse, R., Groot, H., van Kruijsdijk, C., Hajibeygi, H., 2019. Incomplete mixing in porous media: Todd-longstaff upscaling approach versus a dynamic local grid refinement method. Computational Geosciences 23, 373–397. doi:10.1007/s10596-018-9802-0.

[17] Cusini, M., van Kruijsdijk, C., Hajibeygi, H., 2016. Algebraic dynamic multilevel (adm) method for fully implicit simulations of multiphase flow in porous media. Journal of Computational Physics 314, 60 – 79. URL: http://www.sciencedirect.com/science/article/pii/S0021999116001583, doi:https://doi.org/10.1016/j.jcp.2016.03.007.

[18] Duijn, C.J.v., Eichel, H., Helmig, R., Pop, I.S., 2007. Effective equations for two-phase flow in porous media: the effect of trapping at the micro-scale. Transport in Porous Media 9, 411–428.

[19] E, W., 2011. Principles of Multi-Scale Modeling. Cambridge University Press.

[20] E, W., Engquist, B., 2003. The heterogenous multiscale methods. Commun. Math. Sci. 1, 87–132.

[21] E, W., Engquist, B., Li, X., Ren, W., Vanden-Eijnden, E., 2007. Heterogeneous multiscale methods: a review. Commun. Comput. Phys. 2, 367–450.

[22] Edwards, M., 1996. A higher-order godunov scheme coupled with dynamical local grid refinement for flow in a porous medium. Comput. Methods Appl. Mech Eng. 131, 287–308.

[23] Efendiev, Y., Hou, T.Y., 2009. Multiscale Finite Element Methods: Theory and Applications. Springer.

[24] Faigle, B., Helmig, R., Aavatsmark, I., Flemisch, B., 2014. Efficient multiphysics modelling with adaptive grid refinement using a mpfa method. Computat. Geosci. 18, 625–636.

[25] Hajibeygi, H., Bonfigli, G., Hesse, M., Jenny, P., 2008. Iterative multiscale finite-volume method. J. Comput. Phys. 227, 8604–8621.

[26] Hajibeygi, H., Lee, S.H., Lunati, I., 2012. Accurate and efficient simulation of multiphase flow in a heterogeneous reservoir by using error estimate and control in the multiscale finite-volume framework. SPE Journal 17, 1071–1083.

[27] Henning, P., Ohlberger, M., Schweizer, B., 2015. Adaptive heterogeneous multiscale methods for immiscible two-phase flow in porous media. Computational Geosciences 19, 99–114.

[28] Hornung, U., 1997. Homogenization and Porous Media. volume 6. Springer Science & Business Media.

[29] HosseiniMehr, M., Cusini, M., Vuik, C., Hajibeygi, H., 2018. Algebraic dynamic multilevel method for embedded discrete fracture model (f-adm). Journal of Computational Physics 373, 324 – 345. URL: http://www.sciencedirect.com/science/article/pii/S002199911830456X, doi:https://doi.org/10.1016/j.jcp.2018.06.075.

[30] Hou, T.Y., Wu, X.H., 1997. A multiscale finite element method for elliptic problems in composite materials and porous media. J. Comput. Phys. 134, 169–189.

[31] Jansen, J.D., Brouwer, D., Naevdal, G., Kruijsdijk, C.V., 2005. Closed-loop reservoir management. First Break 23.

[32] Jenny, P., Lee, S.H., Tchelepi, H.A., 2003. Multi-scale finite-volume method for elliptic problems in subsurface flow simulation. J. Comput. Phys. 187, 47–67.

[33] de Moraes, R.J., Hajibeygi, H., Jansen, J.D., 2019. A multiscale

method for data assimilation. Computational Geosciences URL: https://doi.org/10.1007/s10596-019-09839-2, doi:10.1007/s10596-019-09839-2.

[34] Moyner, O., Lie, K.A., 2016. A multiscale restriction-smoothed basis method for high contrast porous media represented on unstructured grids. Journal of Computational Physics 304, 46 – 71. doi:https://doi.org/10.1016/j.jcp.2015.10.010.

[35] Pau, G.S.H., Bell, J.B., Almgren, A.S., Fagnan, K., Lijewski, M.J., 2012. An adaptive mesh refinement algorithm for compressible two-phase flow in porous media. Computat. Geosci. 16, 577592.

[36] Radu, F.A., Kumar, K., Nordbotten, J.M., Pop, I.S., 2017. A robust, mass conservative scheme for two-phase flow in porous media including hölder continuous nonlinearities. IMA Journal of Numerical Analysis 38, 884–920.

[37] Sammon, P.H., 2003. Dynamic grid refinement and amalgamation for compositional simulation. in: SPE Reservoir Simulation Symposium, 21-23 February, The Woodlands, Texas, USA, 2003, SPE paper 79683, , 1–11doi:10.2118/79683-MS.

[38] Schmidt, G., Jacobs, F., 1988. Adaptive local grid refinement and multi-grid in numerical reservoir simulation. J. Comput. Phys. 77, 140–165.

[39] Singh, G., Leung, W., Wheeler, M.F., 2018. Multiscale methods for model order reduction of non-linear multiphase flow problems. Computational Geosciences , 1–19.

[40] Singh, G., Leung, W., Wheeler, M.F., 2019. Multiscale methods for model order reduction of non-linear multiphase flow problems. Computational Geosciences 23, 305–323. doi:10.1007/s10596-018-9798-5.

[41] Szymkiewicz, A., Helmig, R., Kuhnke, H., 2011. Two-phase flow in heterogeneous porous media with non-wetting phase trapping. Transport in Porous Media 86, 27–47.

[42] Tene, M., Wang, Y., Hajibeygi, H., 2015. Adaptive algebraic multiscale solver for compressible flow in heterogeneous porous media. Journal of Computational Physics 300, 679 – 694. URL: http://www.sciencedirect.com/science/article/pii/S0021999115005264, doi:https://doi.org/10.1016/j.jcp.2015.08.009.

[43] Wang, Y., Hajibeygi, H., Tchelepi, H.A., 2014. Algebraic multiscale linear solver for heterogeneous elliptic problems. Journal of Computational Physics 259, 284–303.

[44] Zhou, H., Tchelepi, H.A., 2012. Two-stage algebraic multiscale linear solver for highly heterogeneous reservoir models. SPE J., SPE 141473-PA 17, 523–539.

UHasselt Computational Mathematics Preprint Series

2019

UP-19-08 *H. Hajibeygi, M. Bastidas Olivares, M. HosseiniMehr, I.S. Pop, M.F. Wheeler*, **A benchmark study of the multiscale and homogenization methods for fully implicit multiphase ow simulations with adaptive dynamic mesh (ADM)**, 2019

UP-19-07 *J.W. Both, I.S. Pop, I. Yotov*, **Global existence of a weak solution to unsaturated poroelasticity**, 2019

UP-19-06 *K. Mitra, T. Köppl, I.S. Pop, C.J. van Duijn, R. Helmig*, **Fronts in two-phase porous flow problems: effects of hysteresis and dynamic capillarity**, 2019

UP-19-05 *D. Illiano, I.S. Pop, F.A. Radu*, **Iterative schemes for surfactant transport in porous media**, 2019

UP-19-04 *M. Bastidas, C. Bringedal, I.S. Pop, F.A. Radu*, **Adaptive numerical homogenization of nonlinear diffusion problems**, 2019

UP-19-03 *K. Kumar, F. List, I.S. Pop, F.A. Radu*, **Formal upscaling and numerical validation of fractured flow models for Richards' equation**, 2019

UP-19-02 *M.A. Endo Kokubun, A. Muntean, F.A. Radu, K. Kumar, I.S. Pop, E. Keilegavlen, K. Spildo*, **A pore-scale study of transport of inertial particles by water in porous media**, 2019

UP-19-01 *Carina Bringedal, Lars von Wolff, and Iuliu Sorin Pop*, **Phase field modeling of precipitation and dissolution processes in porous media: Upscaling and numerical experiments**, 2019

2018

UP-18-09 *David Landa-Marbán, Gunhild Bodtker, Kundan Kumar, Iuliu Sorin Pop, Florin Adrian Radu*, **An upscaled model for permeable biofilm in a thin channel and tube**, 2018

UP-18-08 *Vo Anh Khoa, Le Thi Phuong Ngoc, Nguyen Thanh Long*, **Existence, blow-up and exponential decay of solutions for a porous-elastic system with damping and source terms**, 2018

UP-18-07 *Vo Anh Khoa, Tran The Hung, Daniel Lesnic*, **Uniqueness result for an age-dependent reaction-diffusion problem**, 2018

UP-18-06 *Koondanibha Mitra, Iuliu Sorin Pop*, **A modified L-Scheme to solve nonlinear diffusion problems**, 2018

UP-18-05 *David Landa-Marban, Na Liu, Iuliu Sorin Pop, Kundan Kumar, Per Pettersson, Gunhild Bodtker, Tormod Skauge, Florin A. Radu*, **A pore-scale model for permeable biofilm: numerical simulations and laboratory experiments**, 2018

UP-18-04 *Florian List, Kundan Kumar, Iuliu Sorin Pop and Florin A. Radu*, **Rigorous upscaling of unsaturated flow in fractured porous media**, 2018

UP-18-03 *Koondanibha Mitra, Hans van Duijn*, **Wetting fronts in unsaturated porous media: the combined case of hysteresis and dynamic capillary**, 2018

UP-18-02 *Xiulei Cao, Koondanibha Mitra*, **Error estimates for a mixed finite element discretization of a two-phase porous media flow model with dynamic capillarity**, 2018

UP-18-01 *Klaus Kaiser, Jonas Zeifang, Jochen Schütz, Andrea Beck and Claus-Dieter Munz*, **Comparison of different splitting techniques for the isentropic Euler equations**, 2018

2017

UP-17-12 *Carina Bringedal, Tor Eldevik, Øystein Skagseth and Michael A. Spall*, **Structure and forcing of observed exchanges across the Greenland-Scotland Ridge**, 2017

UP-17-11 *Jakub Wiktor Both, Kundan Kumar, Jan Martin Nordbotten, Iuliu Sorin Pop and Florin Adrian Radu*, **Linear iterative schemes for doubly degenerate parabolic equations**, 2017

UP-17-10 *Carina Bringedal and Kundan Kumar*, **Effective behavior near clogging in upscaled equations for non-isothermal reactive porous media flow**, 2017

UP-17-09 *Alexander Jaust, Balthasar Reuter, Vadym Aizinger, Jochen Schütz and Peter Knabner*, **FESTUNG: A MATLAB / GNU Octave toolbox for the discontinuous Galerkin method. Part III: Hybridized discontinuous Galerkin (HDG) formulation**, 2017

UP-17-08 *David Seus, Koondanibha Mitra, Iuliu Sorin Pop, Florin Adrian Radu and Christian Rohde*, **A linear domain decomposition method for partially saturated flow in porous media**, 2017

UP-17-07 *Klaus Kaiser and Jochen Schütz*, **Asymptotic Error Analysis of an IMEX Runge-Kutta method**, 2017

UP-17-06 *Hans van Duijn, Koondanibha Mitra and Iuliu Sorin Pop*, **Travelling wave solutions for the Richards equation incorporating non-equilibrium effects in the capillarity pressure**, 2017

UP-17-05 *Hans van Duijn and Koondanibha Mitra*, **Hysteresis and Horizontal Redistribution in Porous Media**, 2017

UP-17-04 *Jonas Zeifang, Klaus Kaiser, Andrea Beck, Jochen Schütz and Claus-Dieter Munz*, **Efficient high-order discontinuous Galerkin computations of low Mach number flows**, 2017

UP-17-03 *Maikel Bosschaert, Sebastiaan Janssens and Yuri Kuznetsov*, **Switching to nonhyperbolic cycles from codim-2 bifurcations of equilibria in DDEs**, 2017

UP-17-02 *Jochen Schütz, David C. Seal and Alexander Jaust*, **Implicit multiderivative collocation solvers for linear partial differential equations with discontinuous Galerkin spatial discretizations**, 2017

UP-17-01 *Alexander Jaust and Jochen Schütz*, **General linear methods for time-dependent PDEs**, 2017

2016

UP-16-06 *Klaus Kaiser and Jochen Schütz*, **A high-order method for weakly compressible flows**, 2016

UP-16-05 *Stefan Karpinski, Iuliu Sorin Pop, Florin A. Radu*, **A hierarchical scale separation approach for the hybridized discontinuous Galerkin method**, 2016

UP-16-04 *Florin A. Radu, Kundan Kumar, Jan Martin Nordbotten, Iuliu Sorin Pop*, **Analysis of a linearization scheme for an interior penalty discontinuous Galerkin method for two phase flow in porous media with dynamic capillarity effects** , 2016

UP-16-03 *Sergey Alyaev, Eirik Keilegavlen, Jan Martin Nordbotten, Iuliu Sorin Pop*, **Fractal structures in freezing brine**, 2016

UP-16-02 *Klaus Kaiser, Jochen Schütz, Ruth Schöbel and Sebastian Noelle*, **A new stable splitting for the isentropic Euler equations**, 2016

UP-16-01 *Jochen Schütz and Vadym Aizinger*, **A hierarchical scale separation approach for the hybridized discontinuous Galerkin method**, 2016